Dual-band Bandpass Plasmonic Filter Based on Effective Localized Surface Plasmon Resonators

Zixiang Zhou[1], Liangliang Liu[1,2], Xinhua Li[1], Jinrui Shen[1], Guodong Han[3], and Zhuo Li[1]

[1]Key Laboratory of Radar Imaging and Microwave Photonics
Ministry of Education, College of Electronic and Information Engineering,
Nanjing University of Aeronautics and Astronautics, Nanjing 211106, China.

[2]State Key Laboratory of Millimeter Waves,
Southeast University, Nanjing, 210096, China.

[3]The 54th Research Institute of CETC, Shijiazhuang, 050081, China.
Corresponding authors: llliu@nuaa.edu.cn; lizhuo@nuaa.edu.cn

Abstract – A dual-band bandpass plasmonic filter based on quarter-wavelength effective localized surface plasmon resonators (ELSPRs) is proposed in this work. Compared with conventional microstrip resonators, ELSPRs have a larger unloaded quality factor and compact size, which can be flexibly designed. Since the harmonics of quarter-wavelength ELSPRs are located only at odd times of their dominant mode frequency, we can not only miniaturize the filter but achieve excellent out-of-band rejection performance. For demonstration, we design and fabricate a dual-band bandpass plasmonic filter, whose size is only $0.0396\ \lambda_0^2$, the center frequency is 3.1 GHz and 3.6 GHz, and the relative bandwidth is 10.7% and 7.7% respectively. Measurement results show excellent agreement with the simulations. Our results provide a route for realizing ultra-compact and high-performance functional devices for the fifth generation (5G) applications.

Index Terms – dual-band bandpass filter, effective localized surface plasmons, harmonic suppression.

I. INTRODUCTION

In recent years, dual-band and multi-band bandpass filters are in high demand for module miniaturization in modern mobile communication systems. Various dual-band bandpass filter (DBPF) structures have been proposed and implemented. For instance, a substrate-integrated waveguide DBPF [1] with low insertion loss and flattening features was proposed. However, its size is still relatively large, and the return loss is not more than 15 dB. A differential dielectric strip resonator (DSR) filter with a dual-band bandpass was realized by loading a pair of ground bars underneath the traditional half-wavelength DSR with high permittivity [2]. Although the unloaded quality factor (Q_u) of this structure reaches 695, it is not flat and compact enough. Although stepped-impedance resonators (SIRs) are commonly used in the DBPF design [3, 4], their application is limited since the resonance frequencies of different SIRs modes are interrelated. Although great effort has been made for multimode resonators [5-11] in the DBPFs design, improvement in balancing various indicators such as Q_u, insertion loss (IL), and size is still limited.

Recently, a novel effective localized surface plasmon resonator (ELSPR) has been proposed in [12–16]. A simplified half-wavelength ($\frac{\lambda_g}{2}$, λ_g denotes the guide wavelength of the resonator at the center frequency) planar ELSPR was put forward and used as a building block in bandpass filter design. The ELSPR is much smaller compared with the conventional microstrip resonator thanks to the high dielectric constant ceramic used. Additionally, the ELSPR has a much higher quality factor than the conventional microstrip resonator. For conventional BPFs based on parallelly-placed microstrip resonators, most energy is transmitted through the lossy substrate between two adjacent microstrip resonators which would lead to large IL. However, for the ELSPR-based BPF design, the medium between two adjacent ELSPRs is the air, which can greatly decrease the insertion loss. So, in this work, we go one step further and use the quarter-wavelength ELSPRs in the BPF design to further decrease the filter size and suppress even harmonics.

In this paper, based on our recent work on single-bandpass filter design using $\frac{\lambda_g}{2}$ ELSPRs, we propose a DBPF based on quarter-wavelength ($\frac{\lambda_g}{4}$) ELSPRs, which is of compact size, high return loss (RL), low IL, and large Q_u.

II. QUARTER-WAVELENGTH ELSPR

As the number of metal wires decreases from 6 to 2 in Figs. 1 (a)-(c), we can observe that hexapolar
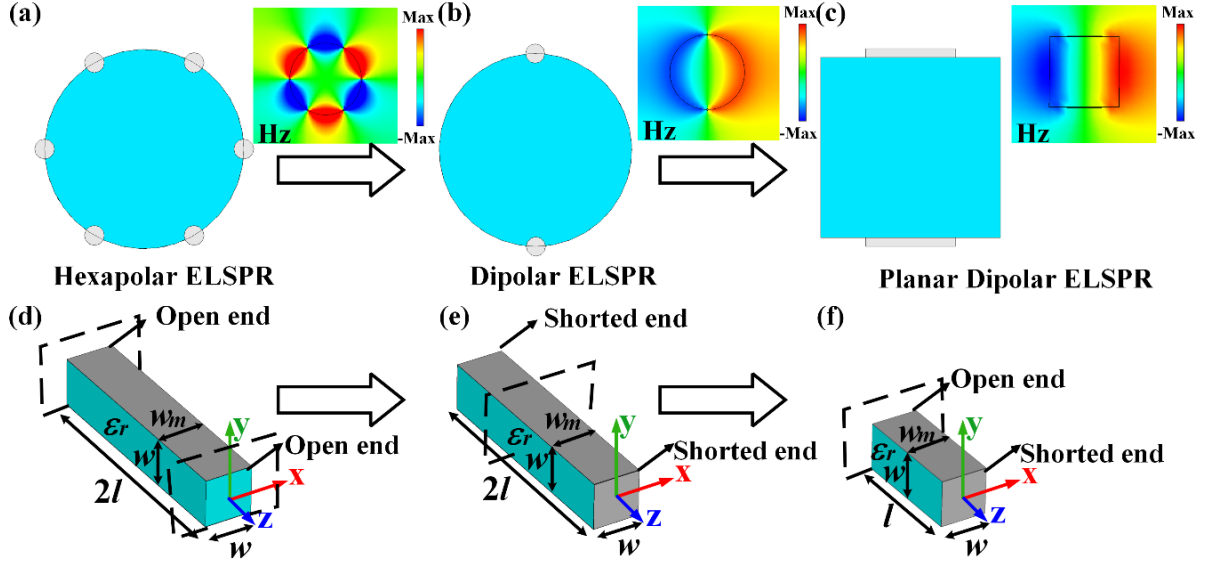
Fig. 1. (a-c) Cross-sectional view and magnetic field distribution of the hexapolar ELSPR, dipolar ELSPR, and planar dipolar ELSPR respectively. (d) A simplified ELSPR with open circuits at both ends. (e) A simplified ELSPR with short circuits at both ends. (f) A $\frac{\lambda_g}{4}$ planar ELSPR with a short circuit at one end and an open circuit at the other end. The 'blue' region denotes the dielectric substrate and the 'grey' part denotes the metal patch.

resonance could not be supported and only dipolar resonance survives. Also, the ELSPR with a rectangular cross-section can be readily fabricated and integrated with planar circuits. Two $\frac{\lambda_g}{2}$ ELSPRs with the same length $2l$ and cross-section dimension are shown in Figs. 1 (d) and (e). The only difference is that the $\frac{\lambda_g}{2}$ ELSPR in Fig. 1 (d) has two open ends and that in Fig. 1 (e) has two shorted ends. However, they have nearly the same resonance frequencies. For further miniaturization, we proposed an $\frac{\lambda_g}{4}$ ELSPR in Fig. 1 (f), which is open at one end and short at the other end. Based on image theory, this $\frac{\lambda_g}{4}$ ELSPR is equivalent to a $\frac{\lambda_g}{2}$ ELSPR in terms of its fundamental mode frequency. According to [15], the fundamental mode frequency of the proposed $\frac{\lambda_g}{4}$ ELSPR can be calculated as:

$$f_a = \frac{c\sqrt{\frac{2}{Re(\varepsilon_r+1)}}}{4l}, \qquad (1)$$

where, c is the speed of light in a vacuum, ε_r is the relative permittivity of the medium, and l is the physical length of the $\frac{\lambda_g}{4}$ planar resonator.

Figures 2 (a) and (b) show the electric field lines of the $\frac{\lambda_g}{4}$ ELSPR at the open and shorted ends, and it can be seen that the ELSPR mode is only located at the open end. For comparison between the $\frac{\lambda_g}{2}$ and $\frac{\lambda_g}{4}$ ELSPRs, we consider in Fig. 2 the evolution of the dipolar mode's resonance frequency and quality factor with the variations of the resonator's dimensions. In Fig. 2 (c), we observe

that the resonance frequencies of both $\frac{\lambda_g}{2}$ and $\frac{\lambda_g}{4}$ ELSPRs decrease with increasing length l when the metal width $w_m = 0.5mm$ is kept constant and is insensitive to the variations of the side length w. In Fig. 2 (d), for both ELSPRs, the Q_u increases with the increase of w_m when w is fixed and the length $l = 10mm$ is kept constant. We also observe in Fig. 2 (e) that the Q_u of both the two resonators decreases with the increase of the length l while the side length $w = 2mm$ and metal width $w_m = 2mm$ are kept constant. In contrast, the $\frac{\lambda_g}{4}$ ELSPR has a lower Q_u than the $\frac{\lambda_g}{2}$ one due to the increasing metallic loss at the shorted end. In Fig. 2 (f), we also compare the mode frequency distributions for both $\frac{\lambda_g}{2}$ and $\frac{\lambda_g}{4}$ ELSPRs with the same fundamental mode frequency at 3.3GHz. It is obvious that the $\frac{\lambda_g}{4}$ ELSPR has resonances located only at odd times of its fundamental mode frequency. For clearance, the resonance frequencies and Q_u of the first five modes for the $\frac{\lambda_g}{2}$ ELSPR and the first three modes of the $\frac{\lambda_g}{4}$ ELSPR are calculated and listed in Table 1. In the next section, the $\frac{\lambda_g}{4}$ ELSPR is used as a basic unit in the DBPF design.

III. DUAL-BAND BANDPASS FILTER BASED ON PLANAR $\frac{\lambda_g}{4}$ ELSPR

A. Design of single-band $\frac{\lambda_g}{4}$ bandpass filter

In general, to implement a DBPF, one should first design two third-order single bandpass filters separately and then combine them by using T-junctions. For the
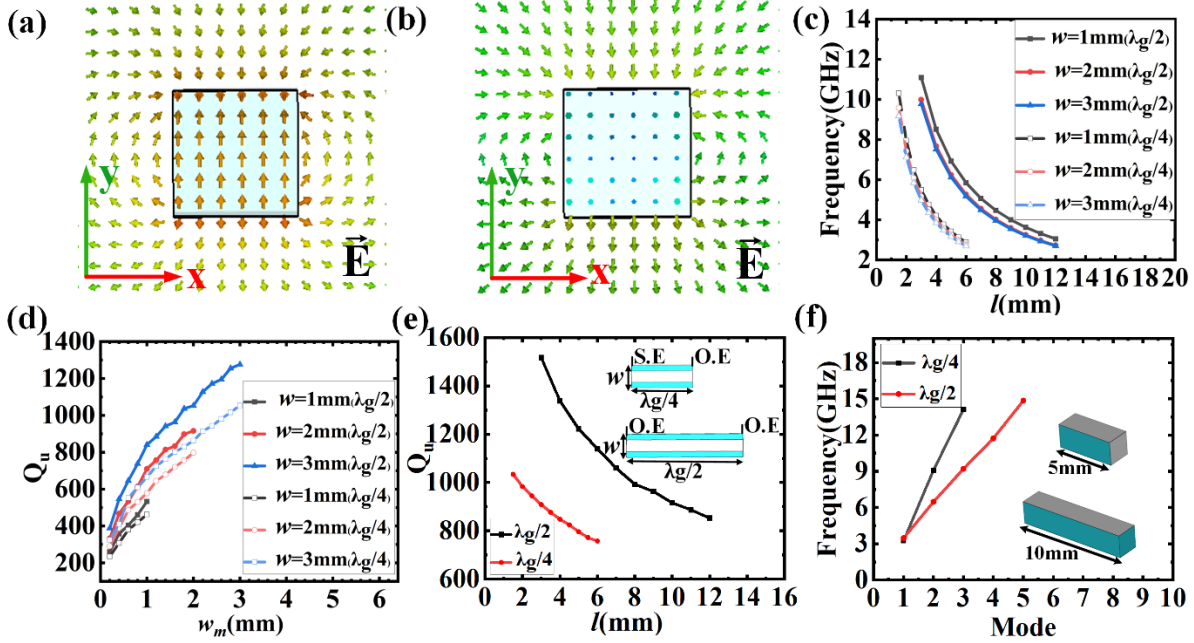
Fig. 2. (a) and (b) Electric field line distributions at the open and shorted end respectively. (c) Evolution of the resonance frequencies of ELSPRs with different l and w. (d) Evolution of Q_u with the variation w_m. (e) Evolution of Q_u with the variation l. (f) Evolution of the resonance frequencies of the $\frac{\lambda_g}{4}$ and $\frac{\lambda_g}{2}$ planar ELSPRs with mode number.

Table 1: Comparison of the resonance modes and the corresponding Q_u of the $\frac{\lambda_g}{2}$ and $\frac{\lambda_g}{4}$ planar ELSPRs

	Mode 1		Mode 2		Mode 3		Mode 4		Mode 5	
	f_0	Q_u	f_0	Q_u	f_0	Q_u	f_0	Q_u	f_0	Q_u
$\frac{\lambda_g}{2}$	3.46	809	6.47	1152	9.20	1418	11.73	1650	14.85	1222
$\frac{\lambda_g}{4}$	3.26	797	9.09	1353	14.12	1771	/	/	/	/

low 5G band or sub-6GHz (450MHz-6GHz) application, two representative center frequencies of 3.1GHz and 3.6 GHz are employed respectively for the design of the proposed ELSPRs. For each ELSPRs-based bandpass filter, the same design framework is shown in Fig. 3 (a), in which three $\frac{\lambda_g}{4}$ ELSPRs are parallelly placed to realize the band-pass filtering function through their mutual coupling. Hereinafter, to better understand the overall design process of the ELSPRs-based filter, we take the central operating frequency of 3.6 GHz as an example and list the design steps of the single bandpass plasmonic filter as follows (we remark that the design in our work can cope with various design requirements, and the operating frequencies can be flexibly tuned by changing the ELSPRs' geometry):

Step 1: Given design specifications as:

1. Center frequency: $f_0 = 3.6$ GHz ;
2. Relative bandwidth: FBW=7.7% ;
3. RL > 20 dB ;

4. IL < 1 dB.

Step 2: Select a three-pole Chebyshev low-pass filter prototype with a bandpass ripple of 0.1 dB. With the normalized low-pass cutoff frequency $\Omega_c = 1$, the low-pass prototype parameters are $g0 = 1$, $g_1 = 1.0316$, $g_2 = 1.1474$, $g_3 = 1.0316$, and $g_4 = 1$, respectively. Thus, we can determine the coupling coefficients and external quality factor (Q_e) as [17]:

$$M_{12} = M_{23} = \frac{FBW}{\sqrt{g_2 g_3}} = 0.071, \qquad (2)$$

$$Q_e = \frac{g_0 g_1}{FBW} = 13.4. \qquad (3)$$

Step 3: A Ceramic material with a relative permittivity of 12.3 and loss tangent of 2.36×10^{-4} is selected as the material of the resonator. Silver is deposited on the top and bottom of the dielectric as well as on the short end. The substrate is made of Rogers RT5880 with a thickness of 0.508 mm. Thus, the ELSPR's length is 9.5 mm according to Eq. (1).
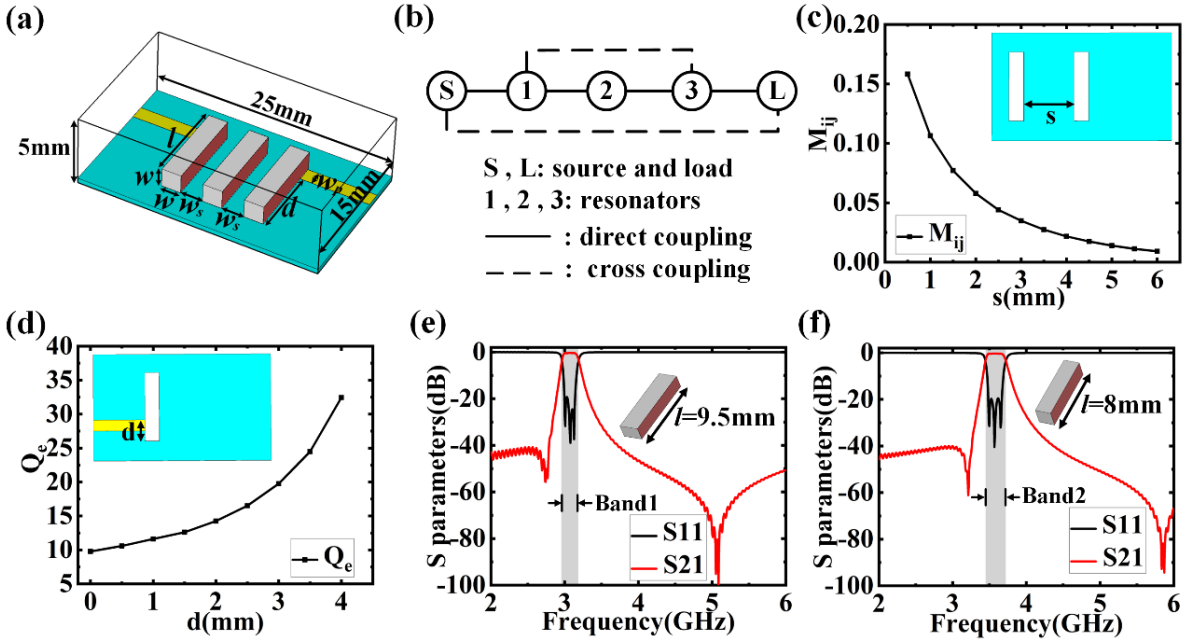
Fig. 3. A Single BPF based on $\frac{\lambda_g}{4}$ planar ELSPR. (a) Schematic diagram of the BPF. (b) Coupling routes. (c) Coupling coefficient between two adjacent ELSPRs. (d) The calculated Q_e of the BPF. (e) and (f) S-parameters of filter I and II with passband Band 1 and Band 2 respectively.

Table 2: Design parameters of single BPF based on $\frac{\lambda_g}{4}$ planar ELSPR

f_0	l	w	w_s	d	w_p
3.1	9.5mm	2mm	2.2mm	7.9mm	1.54mm
3.6	8mm	2mm	2.1mm	7.3mm	1.54mm
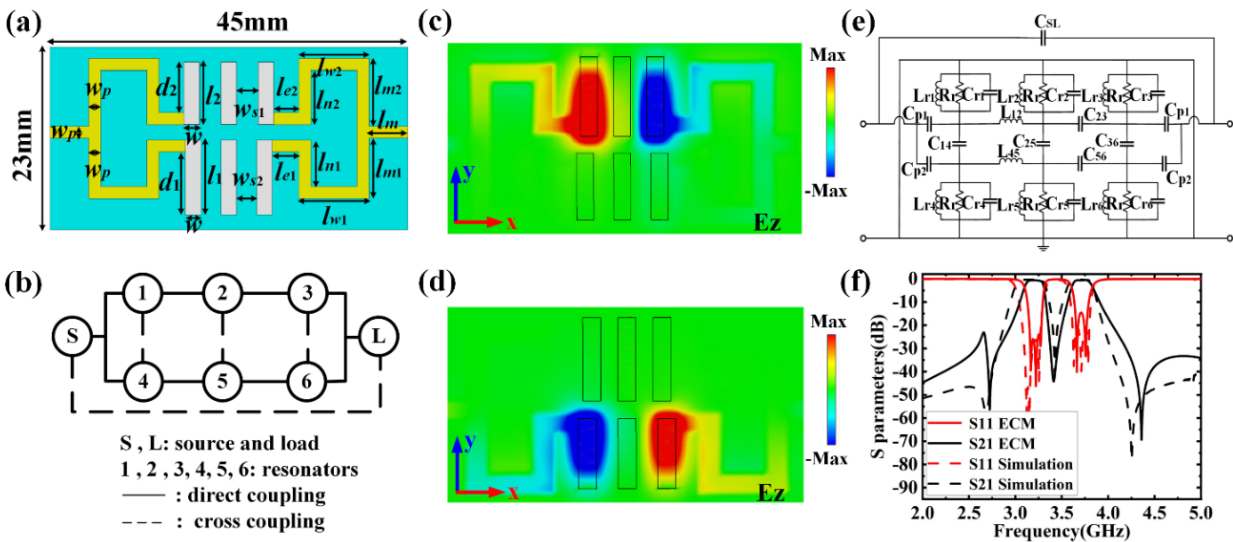
Fig. 4. (a) Layout of the proposed DBPF based on $\frac{\lambda_g}{4}$ ELSPR. (b) Coupling routes. (c) and (d) Distributions of the electric field z-component at the center frequency of 3.1GHz and 3.6GHz respectively. (e) ECM of the proposed DBPF. (f) S-parameters comparison between the ECM simulation in Advanced Design System and CST simulations.

Table 3: Design parameters DBPF based on $\frac{\lambda_g}{4}$ planar ELSPRs

l_1	l_2	w	w_{s1}	w_{s2}	d_1	d_2	w_p	lm
9.5mm	8.0mm	2.0mm	2.1mm	1.8mm	8.0mm	6.5mm	1.54mm	5.0mm
l_{m1}	l_{m2}	l_{w1}	l_{w2}	l_{n1}	l_{n2}	l_{e1}	l_{e2}	
8.3mm	8.5mm	9.1mm	9.1mm	6.0mm	7.0mm	3.5mm	4.7mm	

Table 4: ECM elements for the miniaturized DBPF

L_{r1}	L_{r2}	L_{r3}	L_{r4}	L_{r5}	L_{r6}	L_{12}	L_{45}
0.204nH	0.174 nH	0.313 nH	0.215 nH	0.198 nH	0.217 nH	2.6 nH	3.443 nH
C_{r1}	C_{r2}	C_{r3}	C_{r4}	C_{r5}	C_{r6}	C_{23}	C_{56}
9.05pF	9.981 pF	6.8pF	11.71 pF	9.46 pF	8.031 pF	2.119 pF	1.138 pF
R_r	C_{14}	C_{25}	C_{36}	C_{SL}	C_{p1}	C_{p2}	
0.01Ω	0.385 pF	1.495 pF	1.69 pF	0.025 pF	5.544 pF	11.6 pF	

Step 4: Find the evolution curve in Fig. 3 (c) of the coupling coefficient M_{ij} between Resonators i and j (i, j = 1, 2, 3; 4, 5, 6) with the variation of coupling distance s by using the eigenmode solver in CST, in which M_{ij} can be extracted from the following relationship [18]:

$$M_{ij} = \frac{f_{p2}^2 - f_{p1}^2}{f_{p2}^2 + f_{p1}^2}, \quad (4)$$

where f_{p1} and f_{p2} indicates the two split resonance frequencies of the two parallelly-coupled ELSPRs. Find the evolution curve in Fig. 3 (d) of the Q_e with the variation of feeding position d by using the eigenmode solver in CST, in which Q_e can be extracted by [19]:

$$Q_e = \frac{\omega_0}{\Delta\omega \pm 90°}, \quad (5)$$

where ω_0 is the resonance angular frequency and $\Delta\omega \pm 90°$ is determined by the absolute bandwidth corresponding to the actual phase variation of $90°$ at ω_0.

Determine the initial value of $s = 1.7mm$ by fitting the value from Eq. (2) in Fig. 3 (c) and the initial value of $d = 1.7mm$ by fitting the value from Eq. (3) in Fig. 3 (d).

Step 5: Optimize the S-parameters of the filter by fine-tuning s and d. Finally, the expected design specifications are achieved and shown in Fig. 3 (e), in which the center frequency is 3.1GHz, the relative bandwidth is 10.7%, and the RL is greater than 23dB. Figure 3 (f) shows the S-parameter of the other single pass-band filter with the center frequency at 3.6 GHz and relative bandwidth of 7.7%. The corresponding optimized structural parameters are listed in Table 2.

B. Design of DBPF based on $\frac{\lambda_g}{4}$ ELSPR

We then designed a DBPF by introducing two T-junctions at the input and output ports and combining the above two third-order single-band bandpass filters. The electrical length of the two microstrip lines connecting the T-junction and the side resonator in one bandpass filter is about $\frac{\lambda_g}{4}$ corresponding to the passband central frequency of the other one. Thus, the coupling between these two filters can be minimized. Figures 4 (a) and (b) show the layout of our proposed ELSPRs-based DBPF and its corresponding coupling route, respectively. Figures 4 (c) and (d) show the distributions of the z-component of the electric fields at the two passband center frequencies of 3.1 GHz and 3.6 GHz respectively. It is seen that the two passbands have very high isolations. After optimizations in CST, the final structural dimensions in Fig. 4 (a) can be obtained and listed in Table 3.

C. Equivalent circuit model

To facilitate the understanding of the mechanism of the ELSPs-based DBPF, we give the corresponding model of the equivalent circuit model (ECM) in Fig. 4 (e). A parallel RLC circuit consisting of equivalent inductance L_{ri}, capacitance C_{ri}, and resistance R_r can be used to represent the ELSPR. L_{ij} and C_{ij} represent the electrical coupling between two adjacent resonators. C_p indicates port coupling. C_{SL} indicates the electrical cross-coupling between the load and source. The ECM elements in Fig. 4 (e) are listed in Table 4 in Fig. 4 (f), the corresponding S-parameters derived from the ECM in Advanced Design System and the simulations in CST are compared. Good consistency between these two curves indicates that ECM can be reasonable to describe the DBPF.

D. Fabrication and measurement

Figure 5 (a) shows a picture of the fabricated DBPF, in which the circuit is encapsulated in a height of 5mm aluminum shielding box. Two SMA coaxial connectors are used for the signal input and output. The S-parameters are measured by using the Agilent N5230C vector network analyzer. Figure 5 (b) shows excellent agreement between the simulated and measured S-parameters. The two passbands center at 3.1 GHz and 3.6 GHz and the relative bandwidths are about 10.7% and 7.7%. The insertion losses are less than 0.8 dB

Table 5: Performance comparison between the proposed ELSPR-based DBPF and other DBPFs in previous works

Reference	f_0 (GHz)	IL(dB)	RL(dB)	FBW	Filter Size
[1]	3.5/5.24	1.52/1.65	15/15	2.86%/3.81%	$1.5129\lambda_0^2$
[3]	2.45/5.8	1.8/3.0	10/10	12%/7%	$0.0452\lambda_0^2$
[8]	2.4/5.2	0.6/1.4	12/12	13.7%/6.3%	$0.1932\lambda_0^2$
[20]	2.4/5.2	3.6/3.1	15/23	5.8%/6.4%	$0.0240\lambda_0^2$
[21]	4.32/5.52	2.79/2.92	27.8/25.6	5.76%/4.98%	$0.0635\lambda_0^2$
This work	**3.1/3.6**	**0.53/0.75**	**20/20**	**10.7%/7.7%**	**$0.0396\lambda_0^2$**
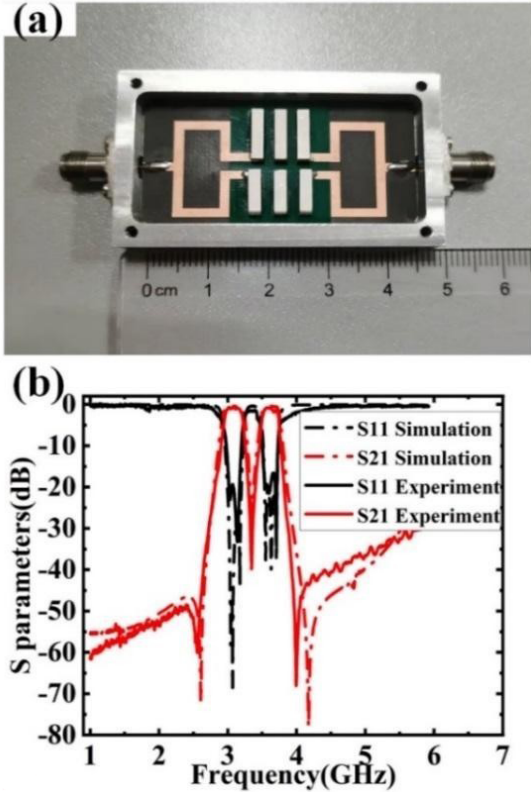
Fig. 5. (a) The fabricated DBPF. (b) Simulated and measured S-parameters.

and the return losses are higher than 20 dB in both pass bands. The upper stopband rejection is greater than 20 dB over a wide frequency range from 4 to 6 GHz. The electrical size of the DBPF is approximately $0.0396 \lambda_0^2$. Compared with published DBPFs in [1, 3, 8, 20, 21] in Table 5 (λ_0 denotes the free-space wavelength at the center frequency). It is seen that the proposed ELSPRs-based DBPF features an excellent balance among various indices including IL, RL, size, and bandwidth.

IV. CONCLUSION

In this work, we explore the characteristics of $\frac{\lambda_g}{4}$ ELSPR and design a compact DBPF by using $\frac{\lambda_g}{4}$ planar ELSPR to suppress even-order harmonics. Simula-

tion and measurement results show that the DBPF can achieve an ultra-compact size, easy integration, low insertion loss, high selectivity, and wide out-of-band rejections. Our design provides a new route to design compact DBPFs and has potential applications in 5G communication systems.

REFERENCES

[1] P. Li, H. Chu, D. Zhao, and R. S. Chen, "Compact dual-band balanced SIW bandpass filter with improved common-mode suppression," *IEEE Microwave and Wireless Components Letters*, vol. 27, no. 4, pp. 347-349, 2017.

[2] Z. Tan, Q.-Y. Lu, and J.-X. Chen, "Differential dual-band filter using ground bar-loaded dielectric strip resonators," *IEEE Microwave and Wireless Components Letters*, vol. 30, no. 2, pp. 148-151, 2020.

[3] J.-T. Kuo, T.-H. Yeh, and C.-C. Yeh, "Design of microstrip bandpass filters with a dual-passband response," *IEEE Trans. Microwave Theory Techniques*, vol. 53, no. 4, pp. 1331–1337, Apr. 2005.

[4] B. Wu, C.-H. Liang, Q. Li, and P.-Y. Qin, "Novel dual-band filter incorporating defected SIR and microstrip SIR," *IEEE Microwave and Wireless Components Letters*, vol. 18, no. 6, pp. 392–394, Jun. 2008.

[5] J. Xu, W. Wu, and C. Miao, "Compact and sharp skirts microstrip dual-mode dual-band bandpass filter using a single quadruple-mode resonator (QMR)," *IEEE Trans. Microwave Theory and Techniques*, vol. 61, no. 3, pp. 1104-1113, 2013.

[6] S. Sun, "A dual-band bandpass filter using a single dual-mode ring resonator," *IEEE Microwave and Wireless Components Letters*, vol. 21, no. 6, pp. 298-300, 2011.

[7] S. Fu, B. Wu, J. Chen, S.-J. Sun, and C.-H. Liang, "Novel second-order dual-mode dual-band filters using capacitance loaded square loop resonator," *IEEE Trans. Microwave Theory and Techniques*, vol. 60, no. 3, pp. 477-483, 2012.

[8] Y. C. Li, H. Wong, and Q. Xue, "Dual-mode dual-band bandpass filter based on a stub-loaded patch resonator," *IEEE Microwave and Wireless Components Letters*, vol. 21, no. 10, pp. 525-527, 2011.

[9] L. Gao, X. Y. Zhang, and Q. Xue, "Compact tri-band bandpass filter using novel eight-mode resonator for 5G WiFi application," *IEEE Microwave Wireless Components Letters.*, vol. 25, no. 10, pp. 660–662, Oct. 2015.

[10] Z. Liu, G. Xiao, and L. Zhu, "Triple-mode bandpass filters on CSRR-loaded substrate integrated waveguide cavities," *IEEE Trans. Components, Packaging and Manufacturing Technology*, vol., 6, no. 7, pp. 1099–1105, Jul. 2016.

[11] S.-W. Wong, S.-F. Feng, L. Zhu, and Q.-X. Chu, "Triple-and quadruple mode wideband bandpass filter using simple perturbation in single metal cavity," *IEEE Trans. Microwave Theory and Techniques*, vol. 63, no. 10, pp. 3416–3424, Oct. 2015.

[12] C. Della Giovampaola and N. Engheta, "Plasmonics without negative dielectrics," *Physical Review. B, Condensed Matter and Materials Physics*, vol. 93, no. 19, May 2016, Art. no. 195152.

[13] Z. Li, L. L. Liu, H. Y. Sun, Y. H. Sun, C. Q. Gu, X. L. Chen, Y. Liu, and Y. L, "Effective surface plasmon polaritons induced by modal dispersion in a waveguide," *Physical Review Applied*, vol. 7, no. 4, pp. 044028, Apr. 2017.

[14] Z. Li, L. L. Liu, A. I. Fernandez-Dominguez, J. F. Shi, C. Q. Gu, F. J. Garcia-Vidal, and Y. Luo, "Mimicking localized surface plasmons with structural dispersion," *Advanced Optical Materials*, vol. 7, no. 10, 2019.

[15] Q. Jiang, Y. Yu, Y. Zhao, Y. Zhang, L. Liu, and Z. Li, "Ultra-compact effective localized surface plasmonic sensor for permittivity measurement of aqueous ethanol solution with high sensitivity," *IEEE Trans. Instrumentation and Measurement*, vol. 70, pp. 1-9, 2021.

[16] Y. Yu, L. Liu , Q. Jiang, Y. Zhao, Y. Zhang, Y. Luo, C. Gu, and Z. Li, "Ultracompact effective localized surface plasmonic bandpass filter for 5G applications," *IEEE Trans. Microwave Theory and Techniques*, vol. 69, no. 4, pp. 2220-2228, 2021.

[17] J.-S. Hong and M. J. Lancaster, "Cross-coupled microstrip hairpin-resonator filters" *IEEE Trans. Microwave Theory and Techniques*, vol. 46, no. 1, pp. 118-122, 1998.

[18] J.-S. Hong and M. J. Lancaster, "Couplings of microstrip square open-loop resonators for cross-coupling planar microwave filters" *IEEE Transactions on Microwave Theory and Techniques*, vol. 44, no. 12, pp. 2099-2108, 1996.

[19] J.-S. Hong and M. J. Lancaster, *Microstrip Filters for RF/Microwave Applications*. Wiley, New York, NY, USA, 2011.

[20] S. Xu, K. Ma, F. Meng, and K. S. Yeo, "Novel defected ground structure and two-side loading scheme for miniaturized dual-band SIW bandpass filter designs," *IEEE Microwave and Wireless Components Letters*, vol. 25, no. 4, pp. 217-219, 2015.

[21] H.-Y. Gao, Z.-X. Tang, X. Cao, Y.-Q. Wu, and B. Zhang, "Compact dual-band SIW filter with CSRRS and complementary spiral resonators," *Microwave and Optical Technology Letters*, vol. 58, no. 1, pp. 1-4, 2016.

Zixiang Zhou was born in Benxi, Liaoning, China, in 1998. She received her B.S. degree in Electronic Information Science and Technology from Nanjing University of Aeronautics and Astronautics (NUAA) in 2020. She is currently pursuing an M.E. degree at NUAA. Her current research interests include effective localized surface plasmons and filters.

Liangliang Liu (M'17) received a B.S. degree in information engineering, an M.E. degree in Electromagnetic Field and Microwave Technology, and Ph.D. degree in Communication and Information System from Nanjing University of Aeronautics and Astronautics (NUAA), China, in 2010, 2013, and 2017, respectively. From Mar. 2017 to Nov. 2020, he joined Nanjing University of Information Science and Technology as an associate professor. From Nov. 2017 to Oct. 2019, he worked at Nanyang Technological University, Singapore, as a Research Fellow. He is currently an associate professor with the College of Electronic and Information Engineering at NUAA. He has published over 60 papers in international refereed journals and conference proceedings. His current research interests include microwave and millimeter-wave devices and antennas, spoof surface plasmons, effective surface plasmons, and coding metasurface.

Xinhua Li was born in Chifeng, Inner Mongolia, China, in 1997. She received her B.S. degree in Information Engineering from Nanjing University of Aeronautics and Astronautics (NUAA) in 2019. She is currently pursuing an M.S. degree at NUAA. Her current research interests include spoof localized surface plasmonic skyrmions and sensors.

Jinrui Shen was born in Pingliang, Gansu, China in 1998. She received her B.S. degree in Electronic Information Science and Technology from Nanjing University of Aeronautics and Astronautics (NUAA) in 2020. She is currently pursuing an M.E. degree at NUAA. Her current research interests include spoof magnetic localized surface plasmons.

Guodong Han was born in Shandong Province, China, in 1980. He received a B.S. degree in Electronic Engineering from the Nanjing University of Aeronautics and Astronautics, Jiangsu, China, in 2003, and M.S. and Ph.D degrees in Electromagnetic and Microwave Technology from the Nanjing University of Aeronautics and Astronautics, Jiangsu, China, in 2005 and 2008, respectively.

From 2008 to 2011, he has been worked at Nanjing Research Institute of Electric Institute (NRIET), Jiangsu, China, as a primary engineer. His work is focused on the active phased array antenna systems in radar. From 2011 to 2013, he completed his postdoctoral work studying the active phased array in the satellite communication field at the 54th Research Institute of China Electronics Technology Group Corporation. Since 2013, he has been involved in the development ofactive/passive antenna system for satellite communication. His research interests include active phased array antenna systems and active components in the RF and microwave frequencies. He has published more than 30 contributory papers in referred journals and international conference proceedings. His team has developed S-band, Ku-band, and Ka-band phased array antennas for satellite communications, which have been applied to mobile platforms such as airborne, vehicular and shipborne. His team has also developed phased array antennas for spaceborne platforms.

Zhuo Li was born in Wuhan, China, in 1979. He received a B.S. degree in Electronic Engineering and an M.E. degree in Electromagnetic Fields and Microwave Techniques from Nanjing University of Aeronautics and Astronautics (NUAA), Nanjing, China, in 2001 and 2004, respectively, and a Ph. D. degree in Radio Engineering from the State Key Laboratory of Millimeter Waves, Southeast University, Nanjing, in 2009. From 2015 to 2016, he was a Visiting Scholar with the Department of Physics at Arizona State University, Tempe, AZ, USA. He is currently a Full Professor at the College of Electronic and Information Engineering at NUAA. He has authored or co-authored over 120 papers in refereed journals and conference proceedings, including Advanced Science, Advanced Optical Materials, Nano Letters, Physical Review Applied, IEEE Transactions on Microwave Theory and Techniques, IEEE Transactions on Antennas and Propagation, and IEEE Transactions on Electromagnetic Compatibility. His current research interests include plasmonic metamaterials, computational electromagnetics, electromagnetic compatibility in avionics and auto-electrical systems.

Prof. Li is an IEEE member, a Senior Member of the Chinese Institute of Electronics and a Committee Member of the Antenna Branch of the Chinese Institute of Electronics.